

# A Dynamic Network for Cryptocurrencies\*

Li Guo<sup>†</sup>

School of Economics, Fudan University

Shanghai Institute of International Finance and Economics

Yubo Tao<sup>‡</sup>

School of Economics, Singapore Management University

Wolfgang Karl Härdle<sup>§</sup>

Center for Applied Statistics and Economics, Humboldt-Universität zu Berlin

Sim Kee Boon Institute for Financial Economics, Singapore Management University

Wang Yanan Institute for Studies in Economics, Xiamen University

Department of Mathematics and Physics, Charles University

December 15, 2021

---

\*Li Guo gratefully acknowledges all participants who attended the workshop “Crypto-Currencies in a Digital Economy” at the Humboldt-Universität zu Berlin for their helpful discussion and comments. Yubo Tao would like to thank Peter C.B. Phillips, Xiaoyi Han, Shuyang Sheng, Liangjun Su, Jun Yu, Yichong Zhang for their insightful suggestions. Wolfgang K. Härdle acknowledges financial support from IRTG 1792 “High Dimensional Non-stationary Time Series”, Humboldt-Universität zu Berlin and that of the Czech Science Foundation under grant no. 19-28231X.

<sup>†</sup>Address: 600 Guoquan Rd, Shanghai 200433. Email: guo\_li@fudan.edu.cn.

<sup>‡</sup>Correspondence author. Address: 90 Stamford Rd, Singapore 178903. Email: ybtao@smu.edu.sg.

<sup>§</sup>Address: Unter den Linden 6 10099 Berlin, Germany. Email: haerdle@hu-berlin.de.

# A Dynamic Network for Cryptocurrencies

## **Abstract**

Cryptocurrencies return cross-predictability yields information on risk propagation and market segmentation. To explore these effects, we build a dynamic network of cryptocurrencies based on the evolution of return cross-predictability and develop a dynamic covariate-assisted spectral clustering method to consistently estimate the latent group membership of cryptocurrencies. We show that return cross-predictability and cryptocurrencies' characteristics, including hashing algorithms and proof types, jointly determine the cryptocurrencies market segmentation. Portfolio analysis reveals that more centered cryptocurrencies in the network earn higher risk premiums.

*JEL Classification:* G11, G12, G41.

*Keywords:* Community Detection, Dynamic Stochastic Blockmodel, Node Covariate, Return Predictability, Network Risk.

# 1 Introduction

The invention of Bitcoin spurred the creation of many cryptocurrencies (cryptos hereafter) commonly known as *Altcoins*. As of December 31, 2018, more than 1500 cryptos are actively traded worldwide, with total market capitalization of more than US\$200 billion. The growing number of Altcoins led investors to investigate inter-relationships between Altcoins to make a profit. However, traditional classification standards applied to equity markets, e.g., Standard Industrial Classification (SIC) and the Global Industry Classification Standard (GICS), fail in cryptos market because they simply focus on fundamental similarities while cryptos with similar mining contracts and business models have completely different ability in generating future cash flows.

To overcome the shortcomings in traditional classification standards, we introduce a novel method to classify financial assets by adding the return cross-predictability to fundamental similarities. On the one hand, return cross-predictability provides timely information to understand the dynamics of market structure and the information propagation across financial assets (Menzly and Ozbas, 2010). On the other hand, the returns embody the investor beliefs which is crucial in classifying cryptos or other hard-to-value financial assets. We naturally employ a directed dynamic network to model the time-varying return cross-predictability and tag the cryptos with the fundamental characteristics (node covariates). By virtue of network analysis, we develop a covariate-assisted spectral clustering (CASC) method that accommodates important network features such as connection sparsity, degree heterogeneity, and directionality, to study the interrelationships between cryptos systematically. We also provide a theory to justify the uniform consistency of our classification method.

In the empirical analysis, we firstly construct a contextualized dynamic directed network of the top 200 cryptocurrencies<sup>1</sup> based on return cross-predictability using a 60-day rolling window adaptive LASSO approach and two most important contract information, i.e., cryptographic algorithm and proof type. Then, we apply our method to estimate the community memberships of each crypto and verify that our methodology can effectively capture the common information of within-group members. In particular, we show that the average return-based and contract-based connections be-

---

<sup>1</sup>The cryptos are ranked by market capitalization as of December 31, 2017.

tween within-group members is significantly higher than that of cross-group members. Lastly, we investigate the portfolio management implication of the crypto clusters. An out-of-sample analysis illustrates that the cryptos from the same group exhibit stronger cross-predictability than those from distinct groups. This evidence indicates that the cross-group asset allocation can achieve a better risk diversification.

Since statistical clustering is usually short of economic interpretations, we also try investigating the economic meaning of the crypto clusters. Specifically, we build a cross-sectional portfolio by sorting on group centrality of the contextualized dynamic network. It is hypothesized that a crypto with more inflow connections (high centrality) tends to receive more shocks from other cryptos, thus bearing a higher risk and leading to higher asset returns. Consistent with this argument, a long-short portfolio of buying cryptos with high centrality and selling cryptos with low centrality earns a significantly positive premium with a portfolio return about 0.4% per day. We further try out other factor for alternative explanations, such as liquidity (Amihud and Mendelson, 1986), investor attention (Liu and Tsvyanski, 2018), and macro uncertainty (Baker et al., 2016). It shows that the excess return of centrality portfolio survives after controlling all of these factors, meaning none of the alternative factors can explain this augmented risk premium.

The present paper makes an important contribution to network analysis in statistics. Specifically, we extend spectral clustering methods to identify communities in dynamic networks in presence of both time-evolving membership and node covariates. In network analysis, community detection is one of the fundamental problems and always faces challenges caused by the features of real data, namely time dependency, degree heterogeneity, sparsity and node covariates, etc.. Numerous methods have been proposed to tackle part of those issues, such as Bhattacharyya and Chatterjee (2017), Pensky and Zhang (2019), and Matias and Miele (2017) for dynamic network models, Wilson et al. (2019) for dynamic degree-corrected stochastic blockmodels, Binkiewicz et al. (2017), Zhang et al. (2016), and Zhang and Rohe (2018) for node covariates in static network models. Fortunately, our proposed community detection method serves as a solution to all the aforementioned data issues and our simulation confirms its superior classification accuracy amongst the state-of-the-art methods.

The paper also deepens the understanding of the cryptos market in terms of both market segmentation and portfolio management. Intensive research in this area considers asset pricing inferences from different angles, but there is limited work that shows the economic link between crypto fundamentals and its performance. Härdle et al. (2020) suggest crypto dynamics as an extraordinary research opportunity for academia and provide some insights into the mechanics of this market. Trimborn et al. (2020) propose a Liquidity Bounded Risk-return Optimization (LIBRO) approach that accounts for liquidity issues by studying the Markowitz framework under liquidity constraints. Hou et al. (2020) propose an option pricing technique for cryptos based on a stochastic volatility model with correlated jumps. Lee et al. (2018) compare cryptos with traditional asset classes and find that cryptos provide additional diversification to mainstream assets, hence improving the portfolio performance. Our results provide new insights into the fundamentals of the cryptos market structure by dividing them into different groups. We find that cryptos' fundamentals have very different features from those of traditional assets, and these features indeed affect a crypto's price evolution.

The remainder of the paper is organized as follows. In section 2, we introduce the model and method to estimate the dynamic group structure and demonstrate the effectiveness of our method via simulation. In section 3, we employ our method to identify the latent group structure of cryptos and provide its portfolio implications. Then, in section 4, we check economic interpretation of the crypto clusters. We conclude in section 5. All proofs and technical details are provided in the supplementary appendix. The R codes to implement the algorithms are available at QuantNet (search keywords “CASC”).

## 2 Models and Methodology

In the equity market, network structures are powerful in revealing risk propagation in assets such as firms, industries, and financial instruments (see, e.g., Cohen and Frazzini, 2008; Aobdia et al., 2014; Acemoglu et al., 2015; Chen et al., 2019a). The latest study, Herskovic (2018), constructs a sector level network based on the Bureau of Economic Analysis (BEA) Input-Output Accounts. Here, we

borrow the network idea to model the inter-dependencies in between cryptos, such as technological similarities and return cross-predictability. However, just applying a network view on cryptos will not give us any insights into the group pattern of the market. We therefore represent the adjacency matrices stochastically via a block structure to identify the latent communities. We base our numerical implementation of this procedure on spectral clustering. [Binkiewicz et al. \(2017\)](#) show that the classification accuracy of the spectral clustering method can be improved by introducing covariate assistance. Here, we present an extension of the covariate-assisted spectral clustering (CASC) algorithm for static undirected networks to deal with the dynamic directed network. The theoretical justifications and simulations both demonstrate the consistency of this method.

## 2.1 Dynamic directed network with covariates

As return predictability between any two cryptos could be mono-directional, we consider a dynamic network defined as a sequence of random directed graphs with  $N$  nodes,  $G_{N,t}$ ,  $t = 1, \dots, T$ , on the vertex set  $V_N = \{v_1, v_2, \dots, v_N\}$ , which does not change over horizons. For each period, we model the directed network structure with an adjacency matrix  $A_t$  which is not necessarily symmetric; that is,

$$A_t(i, j) = \begin{cases} \text{Bernoulli}\{P_t(i, j)\}, & \text{if } i \neq j \\ 0, & \text{if } i = j \end{cases} \quad (1)$$

where  $P_t(i, j) = \Pr\{A_t(i, j) = 1\}$ . The adjacency matrix  $A_t$  records the pattern of edges in the network at time  $t$ ; if there is an edge starting from node  $i \in \{1, \dots, N\}$  and ending at node  $j \in \{1, \dots, N\}$  (i.e.,  $i \rightarrow j$ ), then  $A_t(i, j) = 1$ ; otherwise,  $A_t(i, j) = 0$ . So, the  $i$ th row of  $A_t$  records how node  $i$  sends edges and the  $j$ th column of  $A_t$  records how node  $j$  receives edges.

To reflect the group structure, the probabilities of a connection  $P_t(i, j)$  at period  $t$  are partitioned into blocks. Let the block probability matrix in each period be  $B_t \in [0, 1]^{K_R \times K_C}$  with rank  $K = \min\{K_R, K_C\}$ . In particular, denote  $z_{R,it}$  as the row group label of node  $i$  at time  $t$  and  $z_{C,jt}$  as the column group label of node  $j$  at time  $t$ , respectively; then, if  $z_{R,it} = k_R$  and  $z_{C,jt} = k_C$ , then  $P_t(i, j) = B_t(z_{R,it}, z_{C,jt}) = B_t(k_R, k_C)$ . Hence, for any  $t = 1, \dots, T$ , we can obtain the population

adjacency matrix

$$\mathcal{A}_t \stackrel{\text{def}}{=} \mathbb{E}(A_t) = Z_{R,t} B_t Z_{C,t}^\top, \quad (2)$$

where  $Z_{R,t} \in \{0, 1\}^{N \times K_R}$  and  $Z_{C,t} \in \{0, 1\}^{N \times K_C}$  are the *Row-clustering matrices* and *Column-clustering matrices*, respectively. Notably, there is only one 1 in each row and at least one 1 in each column of each clustering matrix. Co-clustering the adjacency matrix yields two partitions of the same set of nodes. The row clusters contain nodes with similar sending patterns and the column clusters contain nodes with similar receiving patterns.

Zhang and Rohe (2018) showed that the regularization of adjacency matrix can substantially improve the spectral clustering performance, especially for sparse networks. Therefore, we define the regularized graph Laplacian  $L_{\tau,t} \in \mathbb{R}^{N \times N}$  for the directed network as

$$L_{\tau,t} = D_{R,t}^{-1/2} A_t D_{C,t}^{-1/2}, \quad (3)$$

where  $D_{R,t}$  and  $D_{C,t}$  are diagonal matrices with  $D_{R,t}(i,i) = \sum_{j=1}^N A_t(i,j) + \tau_{R,t}$  and  $D_{C,t}(i,i) = \sum_{j=1}^N A_t(j,i) + \tau_{C,t}$ , where  $\tau_{R,t}$  and  $\tau_{C,t}$  are set to be the average row and column degrees at each period, respectively.

We now include the node covariates by constructing a similarity matrix from regularized graph Laplacian  $L_{\tau,t}$  and covariate matrix  $X$ , that is, for each  $t = 1, \dots, T$ ,

$$S_t = L_{\tau,t} + \alpha_t X W_t X^\top = D_{R,t}^{-1/2} A_t D_{C,t}^{-1/2} + \alpha_t X W_t X^\top, \quad (4)$$

where  $\alpha_t \in [0, \infty)$  is the tuning parameter. To employ degree correction, we introduce two sets of degree parameters  $\psi^R = (\psi_1^R, \psi_2^R, \dots, \psi_N^R)$  and  $\psi^C = (\psi_1^C, \psi_2^C, \dots, \psi_N^C)$  such that the edge probability are given by

$$P_t(i,j) = \psi_i^R \psi_j^C B_t(i,j)$$

under the restriction that

$$\sum_{i \in \mathcal{G}_{t,k}^R} \psi_i^R = 1, \forall k \in \{1, 2, \dots, K_R\}, \quad \sum_{i \in \mathcal{G}_{t,k}^C} \psi_i^C = 1, \forall k \in \{1, 2, \dots, K_C\}.$$

Then, the population adjacency matrix for dynamic DCcBM is

$$\mathcal{A}_t = \mathbb{E}(A_t) = \Psi^R Z_{R,t} B_t Z_{C,t}^\top \Psi^C, \quad (5)$$

with  $\Psi^s = \text{Diag}(\psi^s)$ ,  $s \in \{R, C\}$  and the population regularized graph Laplacian is

$$\mathcal{L}_{\tau,t} = \mathcal{D}_{R,t}^{-1/2} \mathcal{A}_t \mathcal{D}_{C,t}^{-1/2}. \quad (6)$$

Therefore, the population similarity matrix is

$$\mathcal{S}_t = \mathcal{L}_{\tau,t} + \alpha_t \mathcal{C}_t^w. \quad (7)$$

where  $\mathcal{C}_t^w = \mathcal{X} \mathcal{W}_t \mathcal{X}^\top$ .

The setup in equation (4) addresses several extensions of existing methods. Firstly,  $W_t$  creates a time-varying interaction between different covariates. For instance, we may think of different refined algorithms that stem from the same origins. Such inheritance relationships will potentially lead to an interaction between the cryptos. In addition, over time, some algorithms may become more popular while the others may near extinction. Thus, this interaction would also change over time. Secondly, we can easily select covariates by setting certain elements of  $W_t$  to zero. This is necessary as it helps us to model the evolution of technologies. At some point in time, some cryptographic technology may be eliminated due to upgrades or cracking. Therefore,  $W_t$  offers us the flexibility to exclude covariates. Lastly, due to the open-source nature of the blockchain, crypto developers can easily copy and paste the source code and launch a new coin without any costs. Consequently, we observe a high degree of homogeneity in the cryptos market. However, this homogeneity does not necessarily result in a cross-predictability of prices: some cryptos are

negatively correlated. In this case, we may set  $W_t(i, i)$  to be negative and  $C_t^w$  will eventually bring the cryptos with different technologies closer in the similarity matrix.

By construction, we know  $D_{R,t}(i, i) = \sum_{j=1}^N \mathbb{1}_{\{i \rightarrow j\}}^{(t)} + \tau_{R,t}$ , which controls for the number of the parents of node  $j$ , and  $D_{C,t}(i, i) = \sum_{j=1}^N \mathbb{1}_{\{j \rightarrow i\}}^{(t)} + \tau_{C,t}$ , which controls the number of the offspring of node  $j$ . To analyze the asymmetric adjacency matrix  $A_t$  caused by directional information, [Rohe et al. \(2016\)](#) propose using the *singular value decomposition* instead of eigen-decomposition for the regularized graph Laplacian. The intuition behind this methodology is to use both the eigenvectors of  $L_{\tau,t}^\top L_{\tau,t}$  and  $L_{\tau,t} L_{\tau,t}^\top$ , which contains information about “the number of common parents” and “the number of common offspring”; that is, for each  $t = 1, \dots, T$ ,

$$(L_{\tau,t}^\top L_{\tau,t})_{ab} = \sum_{i=1}^N L_{\tau,t}(i, a) L_{\tau,t}(i, b) = \frac{1}{\sqrt{D_{C,t}(a, a) D_{C,t}(b, b)}} \sum_{i=1}^N \frac{\mathbb{1}_{\{i \rightarrow a \text{ and } i \rightarrow b\}}^{(t)}}{D_{R,t}(i, i)},$$

$$(L_{\tau,t} L_{\tau,t}^\top)_{ab} = \sum_{i=1}^N L_{\tau,t}(a, i) L_{\tau,t}(b, i) = \frac{1}{\sqrt{D_{R,t}(a, a) D_{R,t}(b, b)}} \sum_{i=1}^N \frac{\mathbb{1}_{\{a \rightarrow i \text{ and } b \rightarrow i\}}^{(t)}}{D_{C,t}(i, i)}.$$

## 2.2 Dynamic covariate-assisted spectral clustering

To set up a dynamic covariate-assisted spectral clustering algorithm, we face two major difficulties: (i) defining  $W_t$  and (ii) estimating the similarity matrix with dynamic network information. For the first issue, we follow [Zhang et al. \(2018\)](#) by setting  $W_t = X^\top L_{\tau,t} X$ , which measures the correlation between covariates along the graph. For the second issue, we follow [Pensky and Zhang \(2019\)](#) by constructing the estimator of  $\mathcal{S}_t$  with a discrete kernel to bring in historical linkage information. Specifically, we first pick an integer  $r \geq 0$ , obtain two sets of integers

$$\mathcal{F}_r = \{-r, \dots, 0\}, \quad \mathcal{D}_r = \{T - r + 1, \dots, T\},$$

and assume that  $|W_{r,l}(i)| \leq W_{\max}$ , where  $W_{\max}$  is independent of  $r$  and  $i$ , and satisfies

$$\frac{1}{|\mathcal{F}_r|} \sum_{i \in \mathcal{F}_r} i^k W_{r,l}(i) = \begin{cases} 1, & \text{if } k = 0, \\ 0, & \text{if } k = 1, 2, \dots, l. \end{cases} \quad (8)$$

Obviously, the  $W_{r,l}$  is a discretized version of the continuous boundary kernel that weighs only the historical observations. This kernel assigns more recent similarity matrices higher scores. To choose an optimal bandwidth  $r$ , Pensky and Zhang (2019) propose an adaptive estimation procedure using Lepski et al. (1997)'s method.<sup>2</sup> Here, we also employ their method and construct the estimator for edge connection matrices:

$$\widehat{\mathcal{S}}_{t,r} = \frac{1}{|\mathcal{F}_r|} \sum_{i \in \mathcal{F}_r} W_{r,l}(i) S_{t+i}. \quad (9)$$

Once we obtain  $\widehat{\mathcal{S}}_{t,r}$ , we create a singular value decomposition of  $\widehat{\mathcal{S}}_{t,r} = \widehat{U}_t \widehat{\Sigma}_t \widehat{V}_t^\top$  for each  $t = 1, 2, \dots, T$ . As Lei and Rinaldo (2015) discuss, the matrix  $\widehat{U}_t$  may now have more than  $K$  distinct rows due to the degree correction, whereas the rows of  $\widehat{U}_t$  still only point to at most  $K$  directions. Therefore, we apply the spherical clustering algorithm to find a cluster structure among the rows of the normalized matrix  $\widehat{U}_t^+$  with  $\widehat{U}_t^+(i, \cdot) = \widehat{U}_t(i, \cdot) / \|\widehat{U}_t(i, \cdot)\|$ . More specifically, we consider the following spherical  $k$ -medians spectral clustering:

$$\left\| \widehat{Z}_{R,t}^+ \widehat{Y}_t - \widehat{U}_t^+ \right\|_F^2 \leq (1 + \varepsilon) \min_{\substack{Z_{R,t}^+ \in \mathcal{M}_{N_+^R, K} \\ Y_t \in \mathbb{R}^{K \times K}}} \left\| Z_{R,t}^+ Y_t - \widehat{U}_t^+ \right\|_F^2 \quad (10)$$

where  $Y_t$  is some rotation matrix. In the last step, we extend  $\widehat{Z}_{R,t}^+$  to obtain  $\widehat{Z}_{R,t}$  by adding  $N - N_+^R$  canonical unit row vectors at the end.  $\widehat{Z}_{R,t}$  is the estimate of  $Z_{R,t}$  from this method. Same techniques applies to  $\widehat{V}_t$  to obtain column clusters. We summarize the algorithm in detail below.

### 2.3 Classification consistency

In the subsequent analysis, we illustrate that the dynamic CASC achieves classification consistency uniformly over time. We first make some assumptions on the graph that generates the dynamic network. The major assumption we need here is *assortativity*, which ensures that the nodes within the same cluster are more likely to share an edge than nodes in two different clusters.

---

<sup>2</sup>See supplementary appendix for detailed dicussion on choosing tunning parameters.

---

**Algorithm 1:** CASC in the Dynamic SC-DCCBM

---

**Input :** Adjacency matrices  $A_t$  for  $t = 1, \dots, T$ ;

Covariates matrix  $X$ ;

Number of row clusters  $K_R$  and number of column clusters  $K_C$ ;

Approximation parameter  $\varepsilon$ .

**Output:** Membership matrices of rows and columns  $Z_{R,t}$  and  $Z_{C,t}$  for  $t = 1, \dots, T$ .

1 Calculate regularized graph Laplacian  $L_{\tau,t}$ .

2 Estimate  $\mathcal{S}_t$  by  $\widehat{\mathcal{S}}_{t,r}$  as in (9).

3 Compute the singular value decomposition of  $\widehat{\mathcal{S}}_{t,r} = \widehat{U}_t \widehat{\Sigma}_t \widehat{V}_t^\top$  for  $t = 1, \dots, T$ .

4 Extract the first  $K$  columns of  $U_t$  and  $V_t$  that correspond to the  $K$  largest singular values in  $\Sigma_t$ , where  $K = \min\{K_R, K_C\}$ . Denote the resulting matrices  $\widehat{U}_t^K \in \mathbb{R}^{N \times K}$  and  $\widehat{V}_t^K \in \mathbb{R}^{N \times K}$ .

5 Let  $N_+^R$  be the number of nonzero rows of  $\widehat{U}_t^K$ ; then, obtain  $\widehat{U}_{t+}^K \in \mathbb{R}^{N_+^R \times K}$  consisting of normalized nonzero rows of  $\widehat{U}_{t+}^K$ ; that is,  $\widehat{U}_{t+}^K(i, \ast) = \widehat{U}_t^K(i, \ast) / \|\widehat{U}_t^K(i, \ast)\|$  for  $i$  such that  $\|\widehat{U}_t^K(i, \ast)\| > 0$ .

6 Similarly, let  $N_+^C$  be the number of nonzero rows of  $\widehat{V}_t^K$ ; then, obtain  $\widehat{V}_{t+}^K \in \mathbb{R}^{N_+^C \times K}$  consisting of normalized nonzero rows of  $\widehat{V}_{t+}^K$ ; that is,  $\widehat{V}_{t+}^K(i, \ast) = \widehat{V}_t^K(i, \ast) / \|\widehat{V}_t^K(i, \ast)\|$  for  $i$  such that  $\|\widehat{V}_t^K(i, \ast)\| > 0$ .

7 Apply the  $(1 + \varepsilon)$ -approximate  $k$ -medians algorithm to cluster the rows (columns) of  $\widehat{\mathcal{S}}_{t,r}$  into  $K_R$  ( $K_C$ ) clusters by treating each row of  $\widehat{U}_{t+}^K$  ( $\widehat{V}_{t+}^K$ ) as a point in  $\mathbb{R}^K$  to obtain  $\widehat{Z}_{R,t}^+$  ( $\widehat{Z}_{C,t}^+$ ).

8 Extend  $\widehat{Z}_{R,t}^+$  and  $\widehat{Z}_{C,t}^+$  to obtain  $\widehat{Z}_{R,t}$  and  $\widehat{Z}_{C,t}$ , respectively, by arbitrarily adding  $N - N_+^R$  and  $N - N_+^C$  canonical unit row vectors at the end, such as  $\widehat{Z}_{R,t}(i) = (1, 0, \dots, 0)$  and  $\widehat{Z}_{C,t}(i) = (1, 0, \dots, 0)$  for  $i$  such that  $\|\widehat{U}_t(i, \ast)\| = 0$  and  $\|\widehat{V}_t(i, \ast)\| = 0$ .

9 Output  $\widehat{Z}_{R,t}$  and  $\widehat{Z}_{C,t}$ .

---

**Assumption 1.** *The dynamic network is composed of a series of assortative graphs that are generated under the stochastic blockmodel with covariates whose block probability matrix  $B_t$  is positive definite for all  $t = 1, \dots, T$ .*

Intuitively, the more frequent the group membership changes, the less stable the network will be. Consequently, it becomes harder to make use of the information from the historical and future network structures to detect the communities in the present network structure. In Assumption 2, we restrict the maximum number of nodes that switch memberships ( $s$ ) to some finite number. Based on this assumption, the proportion of nodes that switch their memberships shrinks to 0 as the size of the network grows to infinity. Additionally, we can easily bound the dynamic behavior of clustering matrices ( $Z_{R,t+r} - Z_{R,t}$  or  $Z_{C,t+r} - Z_{C,t}$ ) by noting that there are at most  $rs$  nonzero rows in the differenced matrix.

**Assumption 2.** *At most,  $s < \infty$  number of nodes can switch their memberships between any consecutive time instances.*

**Assumption 3.** *For  $1 \leq k \leq k' \leq K$ , there exists a function  $f(\cdot; k, k')$  such that  $B_t(k, k') = f(\varsigma_t; k, k')$  and  $f(\cdot; k, k') \in \Sigma(\beta, L)$ , where  $\Sigma(\beta, L)$  is a Hölder class of functions  $f(\cdot)$  on  $[0, 1]$  such that  $f(\cdot)$  are  $\ell$  times differentiable and*

$$|f^{(\ell)}(x) - f^{(\ell)}(x')| \leq L|x - x'|^{\beta - \ell}, \text{ for any } x, x' \in [0, 1], \quad (11)$$

with  $\ell$  being the largest integer smaller than  $\beta$ .

Assumption 3 states that neither the connection probabilities nor the cluster memberships change drastically over the horizons. Lastly, to guarantee the performance of our clustering method, we impose some conditions to regularize the behavior of the covariate matrix and the eigenvalues of the similarity matrices.

**Assumption 4.** *Let  $\lambda_{1,t} \geq \lambda_{2,t} \geq \dots \geq \lambda_{K,t} > 0$  be the  $K = \min\{K_R, K_C\}$  largest singular values*

of  $\mathcal{S}_t$  for each  $t = 1, \dots, T$ . In addition, assume that

$$\underline{\delta}' = \inf_t \left\{ \min_i \{ \min_i \mathcal{D}_{R,t}(i, i), \min_i \mathcal{D}_{C,t}(i, i) \} \right\} > 3 \ln(16NT/\epsilon)$$

and

$$\alpha_{\max} = \sup_t \alpha_t \leq \frac{a}{NRJ^2\xi},$$

with  $a = \sqrt{\frac{3 \ln(16NT/\epsilon)}{\underline{\delta}'}}$  and  $\xi = \max(\sigma^2 \|L_\tau\|_F \sqrt{\ln(TR)}, \sigma^2 \|L_\tau\| \ln(TR), NRJ^2/\underline{\delta}')$ , where  $\sigma = \max_{i,j} \|X_{ij} - \mathcal{X}_{ij}\|_{\phi_2}$ ,  $L_\tau = \sup_t L_{\tau,t}$ .

Following Rohe et al. (2016), we define the “ $R$ -misclustered” and “ $C$ -misclustered” vertices as

$$\mathbb{M}_t^p = \left\{ i: \left\| C_{i,t}^p - \mathcal{C}_{i,t}^p \mathcal{O}_t^p \right\| > \left\| C_{i,t}^p - \mathcal{C}_{j,t}^p \mathcal{O}_t^p \right\|, \text{ for any } j \neq i \right\}, \quad p \in \{R, C\}, \quad (12)$$

where  $C_{i,t}^p$  and  $\mathcal{C}_{i,t}^p$  for  $p \in \{R, C\}$  are the cluster centroids of the  $i$ th node at time  $t$  generated using the  $k$ -medians clustering on the left/right singular vectors and the population left/right singular vectors, respectively.

**Theorem 1.** Assuming  $K_R \leq K_C$  W.L.O.G, let  $Z_{R,t} \in \mathcal{M}_{N,K_R}$ ,  $Z_{C,t} \in \mathcal{M}_{N,K_C}$ , and  $P_{\max} = \max\{\max_{i,t} (Z_{R,t}^\top Z_{R,t})_{ii}, \max_{i,t} (Z_{C,t}^\top Z_{C,t})_{ii}\}$  denote the size of the largest block over the horizons.

Then, under Assumptions 1-3 and 4, the misclustering rate satisfies

$$\begin{aligned} \sup_t \frac{|\mathbb{M}_t^R|}{N} &\leq \frac{c_2(\epsilon) KW_{\max}^2}{m_r^2 N \lambda_{K,\max}^2} \left\{ (6 + c'_w) \frac{b'}{\underline{\delta}'^{1/2}} + \frac{2K_C}{\underline{\delta}'} (\sqrt{2P_{\max}rs} + 2P_{\max}) + \frac{NL}{\underline{\delta}' \cdot \ell!} \left(\frac{r}{T}\right)^\beta \right\}^2, \\ \sup_t \frac{|\mathbb{M}_t^C|}{N} &\leq \frac{c_3(\epsilon) KW_{\max}^2}{m_c^2 N \gamma_c^2 \lambda_{K,\max}^2} \left\{ (6 + c'_w) \frac{b'}{\underline{\delta}'^{1/2}} + \frac{2K_C}{\underline{\delta}'} (\sqrt{2P_{\max}rs} + 2P_{\max}) + \frac{NL}{\underline{\delta}' \cdot \ell!} \left(\frac{r}{T}\right)^\beta \right\}^2, \end{aligned}$$

with a probability of at least  $1 - \epsilon$ , where  $c_2(\epsilon) = 2^6(2 + \epsilon)^2$ ,  $c_3(\epsilon) = 2^7(2 + \epsilon)^2$ ,  $b' = \sqrt{3 \ln(16NT/\epsilon)}$ ,  $\gamma_c$  are defined in supplement equation (S27), and  $\lambda_{K,\max} = \max_t \{\lambda_{K,t}\}$  with  $\lambda_{K,t}$  being the  $K$ th largest absolute singular value of  $\mathcal{S}_t$ .

**Remark 1.** The upper bounds on misclustering rates obtained in the Theorem 1 are non-asymptotic. Assuming that  $s$  is constant and the number of covariates  $R$  grows at  $O(\ln(NT))$  rate, we can obtain

that, as  $N, T \rightarrow \infty$ ,

$$\sup_t \frac{|\mathbb{M}_t^R|}{N} = O_p \left( \frac{\ln(NT)}{NT} \right) \text{ and } \sup_t \frac{|\mathbb{M}_t^C|}{N} = O_p \left( \frac{\ln(NT)}{NT} \right). \quad (13)$$

## 2.4 Monte Carlo simulations

In this section, we carry out several simulation studies using our algorithm and existing clustering methods under different model setups. Our benchmark algorithms for the directed networks are the degree-corrected DI-SIM (DI-SIM-DC) by Rohe et al. (2016) and the covariate-assisted DI-SIM for static networks (CA-DI-SIM-Stc) by Zhang et al. (2018). Since both methods are for static networks, we apply them to the adjacency matrix in each period and report the average misclustering rate over time.

We set the block probability matrix  $B_t$  as

$$B_t = \begin{bmatrix} 0.60 & 0.30 & 0.20 & 0.10 \\ 0.30 & 0.50 & 0.20 & 0.10 \\ 0.20 & 0.20 & 0.40 & 0.10 \\ 0.10 & 0.10 & 0.10 & 0.30 \end{bmatrix} \times \frac{T+2t}{2T}, \text{ with } 1 \leq t \leq T. \quad (14)$$

and set the order of the polynomials for kernel construction at  $L = 4$  for all simulations. Then, we generate the initial clustering matrices  $Z_{R,1}$  and  $Z_{C,1}$  by randomly choosing one entry in each row and assign it to 1. For  $t = 2, \dots, T$ , we fix the last  $N-s$  rows of  $Z_{R,t-1}$  and  $Z_{C,t-1}$  and re-assign 1s in the first  $s$  rows of  $Z_{R,t-1}$  and  $Z_{C,t-1}$ , respectively, to mimic the group membership changes. Lastly, we assume that the number of communities  $K_R = K_C = 4$  for directed network is known throughout the simulations. The time-invariant node covariates are  $R = \lfloor \ln(NT) \rfloor$  dimensional with values  $X \sim U(0, 10)$ . We replicate all experiments 1000 times and the misclustering rate we report is the temporal average of the misclustering rates; that is,  $T^{-1} \sum_{t=1}^T |\mathbb{M}_t^R|/N$  and  $T^{-1} \sum_{t=1}^T |\mathbb{M}_t^C|/N$ .

We first examine the clustering performance with a growing network size. The number of vertices in the network varies from 20 to 200 with step size 20. The time span is  $T = 10$  and the number of membership changes is  $s = 10$ . We summarize the results in Figure 1 (a) and (b). Evidently,

as the size of the network becomes larger, the misclustering rates of the CA-DI-SIM-Dyn decrease sharply and dominate both CA-DI-SIM-Stc and DI-SIM-DC throughout the simulation. The CA-DI-SIM-Stc dominates DI-SIM-DC in classification accuracy, which is consistent with the argument that some similarity is sufficient for the covariates to assist in the discovery of the graph structure. (Binkiewicz et al., 2017). The dominating performance of CA-DI-SIM-Dyn over CA-DI-SIM-Stc proves that historical linkage information is crucial for improving classification accuracy.

[Figure 1 is about here.]

Next, we check the relative performance for a growing maximal number of group membership changes. Here, we fix the total number of vertices at 200 and we vary the group membership changes for each period,  $s$ , from 20 to 100 with step size 20. The total number of horizons is  $T = 10$ . We summarize the results in Figure 1 (c) and (d). Obviously, the misclustering rate of our method increases with the number of group membership changes. The benchmark methods are insensitive to the change of group memberships because they estimate clusters using one-period adjacency matrix. Despite the result, our method still achieves the lowest misclustering rate amongst all methods when the group memberships are relatively stable ( $s < N/2$ ).

To perceptually illustrate the supreme accuracy of the dynamic CASC over the benchmark methods, we visualize the block structure of the dynamic network in Figure 2 by drawing the average adjacency matrices over a certain period and sort the rows and columns according to their group labels. Specifically, we simulate a dynamic network of 200 nodes with 4 blocks across 10 periods according to the block probability matrix  $B_t$  in equation (14) setting parameter values  $s = 10$ ,  $R = \lfloor \ln(NT) \rfloor$ , and  $X \sim U(0, 10)$ . Then we calculate the average adjacency matrix over 6 periods,<sup>3</sup>  $1/6 \sum_{t=1}^6 A_t$ , and sort the rows and columns jointly according to their group labels. Taking the average adjacency matrix as a  $200 \times 200$  grid, we paint the square with a darker color when it has a larger value.

---

<sup>3</sup>We choose 6 periods because the optimal bandwidth  $r$  is chosen as 5 in the simulation. So using 6 periods will lose no information in the kernel.

[Figure 2 is about here.]

Clearly, the graph with true clusters exhibits a clear block structure where each block is associated with reasonable connection frequencies abide by the block probability matrix. All three methods successfully recover the dense blocks (blocks in the northwest corner) whereas only the dynamic CASC is able to recover the sparse blocks (blocks in the southeast corner). The simulation results serves as a remarkable evidence to confirm the advantages of the dynamic CASC in dealing with sparse networks.

### 3 Cryptos Network and Clusters

In this section, we illustrate how we construct a dynamic network structure using crypto returns and its contract information. Specifically, we first form a return-based network using the inter-predictive relations between cryptos. In addition, we add linkages between the cryptos that adopt similar cryptography techniques. We then perform clustering with our new algorithm.

#### 3.1 Data and variables

We collected data on the historical daily prices, trading volumes, and contract attributes of the top 200 cryptos by market capitalization from an interactive platform (*Cryptocompare.com*) with free API access. After excluding cryptos with incomplete contract information, we obtain a sample of 199 cryptos. The sample covers August 31, 2015 to March 31, 2018. In term of the time-invariant attributes, we mainly collected algorithm and proof types from each crypto's contract:

*Algorithm*, which is short for the *hashing algorithm*, plays a central role in determining the security of the crypto. For each crypto, there is a hash function in mining; for example, Bitcoin (BTC) uses double SHA-256 and Litecoin (LTC) uses Scrypt. As security is one of the most important features of cryptos, the hashing algorithm naturally—in terms of trust—determines the intrinsic value of a crypto. In the example above, the Scrypt system was used with cryptos to improve upon the SHA256 protocol. The SHA256 preceded the Scrypt system and was the basis

for BTC. Specifically, Scrypt was employed as a solution to prevent specialized hardware from brute-force efforts to out-mine others. Thus, Scrypt-based Altcoins require more computing effort per unit, on average, than the equivalent coin using SHA256. The relative difficulty of the algorithm confers a relative value.

*Proof Types*, or proof system/protocol, is an economic measure to deter denial of service attacks and other service abuses such as spam on a network by requiring some work from the service requester, usually the equivalent to processing time by a computer. For each crypto, at least one of the protocols will be chosen as a transaction verification method; for example, BTC and Ethereum (ETH) currently use the Proof-of-Work (PoW), and Diamond (DMD) and Blackcoin use the Proof-of-Stake (PoS). PoW-based cryptos such as BTC use mining—the solving of computationally intensive puzzles—to validate transactions and create new blocks. In PoS-based cryptos, the creator of the next block is chosen through various combinations of random selection and wealth (in terms of crypto) or age (i.e., the stake). In summary, the proof protocol determines the reliability, security, and effectiveness of the transactions.

### 3.2 Cryptos network construction

According to the traditional asset pricing theory, a classical view of the cross-predictability of stock returns reflects the correlations in the fundamental determinants caused by common information of the future cash flows or discount rates. Since the cryptos are traded at high frequency, return information is particularly important as it serves as timely information towards understanding the dynamics of market structure. Accordingly, to project the commonality of cryptocurrency community, we first study the return cross-predictability among the top 200 cryptocurrencies according to the market capitalization in the end of 2017.

To select the most informative linkage among cryptocurrencies, we regress a certain cryptocurrency returns on the other cryptos' lagged returns in a 60-day rolling window. In particular, we

employ the adaptive LASSO (Zou, 2006) to estimate the regression coefficient; that is,

$$\hat{b}_i^* = \arg \min \left\{ \left\| r_{i,t+1}^s - \alpha_i - \sum_{j \neq i} b_{i,j} r_{j,t}^s \right\|^2 + \lambda_i \sum_{j \neq i} \hat{w}_{i,j} |b_{i,j}| \right\}, \quad (15)$$

where  $r_{j,t}^s$  is the standardized return for crypto  $j$ ,  $\hat{b}_i^* = (\hat{b}_{i,1}^*, \dots, \hat{b}_{i,N}^*)^\top$  is the adaptive LASSO estimate,  $\lambda_i$  are non-negative regularization parameters, and  $\hat{w}_{i,j}$  are the weights corresponding to  $|b_{i,j}|$  for  $j = 1, \dots, N$  in the penalty term. Conventionally, one defines  $\hat{w}_{i,j} = 1/|\hat{b}_{i,j}^{LS}|^\gamma$  with some  $\gamma > 0$  where  $\hat{b}_{i,j}^{LS}$  denotes the coefficient estimated by ordinary least squares. The LASSO technique yields an active set that has “parental” influence on the focal crypto. Thus, we obtain an adjacency matrix for each period,  $A_t$ ,  $t = 1, \dots, T$ .

In Figure 3, we visualize a subgroup of 20 cryptos on selected dates to illustrate the structural features revealed by (15). Evidently, the return-inferred network is time-varying and sparse in general. Taking subfigures (a) and (d) as an example, the interrelation between BTC and DMD vanishes on January 1, 2018, and the network on January 1, 2018 are sparser than that on January 15, 2018. These observations imply that we may need more information, e.g., node covariates, to help resolve the sparsity issue.

[Figure 3 is about here.]

To demonstrate how cryptos’ contract information assists classification, we replot the network with the same cryptos in Figure 3 and link the cryptos that share at least one fundamental characteristic to obtain Figure 4. For example, LTC and DOGE are linked since they both adopt the Scrypt algorithm. Due to the limited choices of algorithms and proof types, the cryptos are more likely to connect with each other when using attribute commonality to form linkages.

[Figure 4 is about here.]

One would possibly cluster cryptos according to their contract commonalities. However, contract commonality per se is not enough to classify cryptos since it omits the investors’ beliefs,

which is particularly important for the cryptos market, carried in the crypto returns. Actually, the relationship between a crypto's fundamental to its prices is more complicated than a company's fundamental to its equity prices. It is possible that coins with exactly the same fundamentals behave completely different in prices. Take IXCoin, the first BTC *clonecoin*,<sup>4</sup> as an example, even though it copied every detail from Bitcoin, it was unable to replicate the success of BTC. The developers stopped working on IXCoin for months after its initial coin offering (ICO). In fact, a clonecoin could be more risky than its proto-coin for speculation reasons.

To account for both sets of information, we combine the return-based network and the contract-based network such that cryptos can be connect to others either by return cross-predictability or fundamental similarity. Figure 5 illustrates the combined network for selected dates. Compared to the networks based on a single information set, the combined network is denser and the degrees of the cryptos are distributed more evenly. Consequently, classification on the combined network will deliver more accurate clusters.

[Figure 5 is about here.]

### 3.3 Clusters of cryptos network

The combined network structure and application of the dynamic CASC created four groups. Table 1 summarizes the grouping results for one example. The table indicates that as of 2017-12-31, the largest cryptos (BTC, ETH, and LTC) in terms of market capitalization are not necessarily categorized into the same group. Take LTC and BTC as an example. Although their return patterns are closely related, the fundamental attributes between them are rather different: BTC employs SHA256 while LTC uses Scrypt. As a comparison, we also show the grouping results for the same 20 cryptos under DISIM from Rohe et al. (2016) in Table 1.

[Table 1 is about here.]

---

<sup>4</sup>Due to the open-source nature of blockchain, many developers simply copy and paste the blockchain source codes and make minor modifications on the parameters to launch a new coin, which we call it a *Clonecoin*.

To evaluate the accuracy of classification results, we check the differences between the within- and cross-group connections of each group, defined as

$$\begin{aligned} \text{Within-Group Connection}_i &= \frac{\# \text{ of Degrees of Coins within Group } i}{4N_i}, \\ \text{Cross-Group Connection}_i &= \frac{\# \text{ of Degrees of Coins between Group } i \text{ and other Groups}}{4\bar{N}_i}, \end{aligned}$$

where  $N_i$  is the number of cryptos in group  $i$  and  $\bar{N}_i$  is the number of cryptos not in group  $i$ . Intuitively, if the clustering method correctly classifies all cryptos, then the within-group connections should be larger than the cross-group connections; that is, the difference between them should be positive. Table 2 summarizes the within- and cross-group connections of different information sets based on DISIM from [Rohe et al. \(2016\)](#) and dynamic CASC, respectively. Panel A reports the average return-based connection over the sample period. Panels B and C report the algorithm-inferred connections and proof-types-inferred connections, respectively. The differences between the within- and cross-group connection (W-C difference) are reported in the last column of each panel.

[Table 2 is about here.]

Evidently, the dynamic CASC method has superior classification efficiency than DISIM does, as it delivers higher overall differences in both return-inferred connections and contract-inferred connections. For example, the overall W-C difference of DISIM is 0.004, 0.026, and 0.036, while that of dynamic CASC is 0.007, 0.037, and 0.039, respectively. Indeed, dynamic CASC utilizes fundamental information better in the sense that the contract-inferred network structure (Panels B and C) generates a higher W-C difference without discounting the grouping information from the return-inferred network. These facts indicate that fundamental information introduces an extra dimension of commonality for classifying cryptos, and improves the information extraction from return dynamics by emphasizing the return cross-predictability induced by fundamental commonality.

### 3.4 Post-classification portfolio management

Risk diversification is one of the most important issues in portfolio management. Portfolio managers seek to achieve a target return with the smallest variance possible. Therefore, it is crucial to invest in different assets or equity sectors that are not highly correlated with each other. We calculate the correlation coefficients of cryptos within the same group and those of the cryptos across groups out-of-sample. Table 3 summarizes the results.

[Table 3 is about here.]

In Table 3, we compare the average pair-wise correlations between two groups. For the within-group portfolio, we randomly pick 10 cryptos from the same group, and for the cross-group portfolio, we randomly pick 5 cryptos in one group and pick the remaining 5 cryptos from other groups. Then, for each trading day, we balance the portfolio according to the clustering results and calculate the within- and cross-group correlations in the next 60 trading days. Table 3 demonstrates that the correlations between cryptos within the same group are on average significantly higher than those across groups are. Indeed, the average correlation coefficient within a group is 0.18, while it is 0.15 across groups. In economic terms, this result indicates a 17% reduction in return cross-predictability when investing in cross-group cryptos. The difference is statistically significant at the 1% level with a Newey-West adjusted  $t$ -statistic of 6.33. The result suggests that investment practitioners can find attractive upside and diversification possibility through allocating portfolio weights on cryptos from different groups. As buying all cryptos is costly, the findings provide portfolio managers the opportunity to select group representatives with a significant diversification effect.

## 4 Economic Interpretation

In this section, we mainly investigate the economic meanings of the clusters. We argue that the cluster is mainly a reflection of risk propagation. We also present several robustness results to rule out alternative explanations of the centrality measure.

## 4.1 Centrality and crypto returns

[Acemoglu et al. \(2012\)](#) propose a theoretical model to study how risk and trading information propagates from one crypto to another through sector-level shocks. The model suggests that if the linkages in the inter-sectoral network are sufficiently asymmetric, then sectoral shocks might not cancel out through diversification, but aggregate into macroeconomic fluctuations. [Ahern \(2013\)](#) also finds that idiosyncratic shocks could travel between linked stocks following the direction of the linkages. Therefore, stocks with more “receive linkages” tend to bear more risks in the network and thus require a higher risk premium. Similarly, [Barrot and Sauvagnat \(2016\)](#) find the idiosyncratic shocks propagate in production networks. Correspondingly, we would expect that cryptos in a more central position in the network require higher risk premiums.

Centrality, as the key measure describing the importance of the nodes in the network, best proxies the concentration of risks or trading information. There are several measures of centrality, such as degree, closeness, betweenness, and eigenvector centrality. Among them, eigenvector centrality is the most appropriate measure for an asymmetric network for two reasons. First, shocks that transmit across the cryptos market do not have final recipients and are unlikely to follow the shortest path between nodes. Therefore, we cannot use closeness and betweenness centrality to describe market shocks as they implicitly assume that traffic follows geodesic paths ([Borgatti, 2005](#)). Second, cross-asset shocks are likely to have feedback effects evidenced by the two-way connections between paired cryptos in Figure 3. Thus, using degree centrality tends to overestimate the importance of cryptos with more asymmetric linkages. Eigenvector centrality is calculated via the principal eigenvector of the network’s adjacency matrix ([Bonacich, 1972](#)). Nodes are more central if they are connected to other nodes that are themselves more central. Figure 6 plots the average return of each group portfolio, labelled as high-, median- (2 groups in the middle), and low-centrality groups. Based on the thoughts on portfolio performance above, we find that the group with a higher centrality wins the horse race.

[Figure 6 is about here.]

Next, we formally test this discovery by studying cross-sectional portfolio returns. We first sort cryptos into 4 groups based on the eigenvector centrality calculated from the similarity matrix on each trading day. We then look at each portfolio’s average future returns. Next, we test the statistical significance of the difference in average future return between the high and low portfolios. To show the informativeness of our centrality measure, we construct the portfolio for several formation periods, ranging from day  $t + 1$  to  $t + 7$  days. Table 4 reports the results.

[Table 4 is about here.]

In line with the observations from Figure 6, the cryptos with a higher quartile of centrality receive a higher portfolio return. Particularly, the average portfolio return is 39.78 bps for the highest-centrality group, while it is -0.01 bps for the lowest-centrality group. The difference is statistically significant at the 1% level. We find similar results across different portfolio formation periods. The result provides strong evidence that an informational channel, such as risk and liquidity, should be applied to interpret the eigenvector centrality measure.

## 4.2 Alternative interpretation

We showed that the centrality measure is economically meaningful as a risk factor. However, it does not rule out other explanations. We therefore conduct several tests to seek other possibilities to link the centrality measure to economic theory. In particular, we test if limit-to-arbitrage, investor attention, and macroeconomic uncertainty can deliver meaningful explanatory power of the anomaly.

The first typical explanation for asset return anomaly is the limit-to-arbitrage. According to Shleifer and Vishny (1997), sophisticated investors would quickly eliminate any return predictability arising from anomalies in a liquid market without impediments to arbitrage. Therefore, when cryptos are illiquid, an arbitrage opportunity is more likely to exist between central and non-central cryptos. As a formal test, we proxy liquidity with trading volume and first sort the cryptos into two groups (high and low) according to their previous day’s trading volume. Then, for each

group, we sort cryptos by their eigenvector centrality as in the previous sections, and report the corresponding portfolio returns in the first two columns of Table 5.

We find that the centrality portfolio return (High–Low) remains significantly positive for both high- and low-volume cryptos. For example, in the low-volume group, the portfolio return is 5 bps for the low-centrality group, while it increases to 28 bps for the high-centrality group. The significantly positive portfolio returns in both groups indicate that the limit-to-arbitrage does not fully explain the centrality measure.

[Table 5 is about here.]

The recent study of [Liu and Tsyvinski \(2018\)](#) provides an alternative explanation. The authors find that investor attention is a powerful predictor of crypto returns. [Barber and Odean \(2008\)](#) point out that excess attention usually drives investors to overreact to information and thus causes mispricing. [Guo et al. \(2018\)](#) show that investor attention could spill over along the network linkages. Hence, cryptos in a high-investor-attention period are more likely to be mispriced. Following [Liu and Tsyvinski \(2018\)](#), we proxy investor attention by constructing the deviation of Google searches for the word “crypto” on a given day compared to the average of those in the preceding four weeks. We split the sample into two periods (high and low) and test for the existence of the anomaly in each period. We summarize the results in the middle columns of Table 5.

In general, the proposed centrality measure—under both high- and low-attention periods—is a better choice. The effect seems to be stronger in high-attention periods. For example, the centrality portfolio achieves a 0.45% daily return during a high-attention period, while it retains a 0.35% return, if not higher, for the low-attention period. However, we can observe that the results are not fully explained by investor attention, as our centrality measure shows significant cross-sectional return predictability.

Last, observing that government policy and crypto price movement has a strong synchronization ([Demir et al., 2018](#)), we must check whether the centrality measure relates to underlying economic uncertainty. Naturally, when macroeconomic conditions become uncertain, investing in a certain

asset is more risky and investors will require a higher risk premium (Brogard and Detzel, 2015). We employ Baker et al. (2016) policy uncertainty index, which is constructed from three types of underlying components: media news; the Congressional Budget Office (CBO), which compiles lists of temporary federal tax code provisions; and the Federal Reserve Bank of Philadelphia’s Survey of Professional Forecasters. Similarly, we divide the sample into two parts, high- and low-uncertainty periods, and test the existence of abnormal returns in each period. The last two columns of Table 5 report the results.

Evidently, the centrality portfolio return remains significantly positive under both high- and low-economic-uncertainty periods. Specifically, in a high-period, the portfolio return is 1 bps for the low-centrality group and 49 bps for the high-centrality group, which reveals a difference of 48 bps with a Newey-West adjusted  $t$ -statistic of 2.71. The results are a bit weaker in the low-uncertainty period, but the overall pattern remains. In this case, the centrality measure cannot be fully explained by economic uncertainty.

In summary, the proposed centrality measure is not driven by the pricing factors listed above. Although we did not exhaust all possibilities, the facts suggest that the centrality measure serves well as an idiosyncratic risk factor to predict future crypto returns.

## 5 Conclusion

This study examined the market segmentation problem in the cryptos market. To solve the problem, we constructed a dynamic network of cryptos using return inter-predictive relationship and proposed a dynamic CASC method to make full use of the dynamic linkage information, as well as the node attributions, to improve classification accuracy. In virtue of network analysis and in the spirit of Ahern (2013), we proposed using eigenvector centrality as the measure of idiosyncratic risk to predict cryptos’ future returns. We find that the cross-sectional portfolio constructed from eigenvector centrality sorting can deliver a persistent 40 bps daily return.

The current paper mainly focuses on the uniform consistency of the classification method. Recent literature has developed inspiring framework for statistical inference on membership profiles

as well as on estimation of low-rank matrices, e.g. Fan et al. (2019); Chen et al. (2019b). It is an interesting and critical research direction to investigate how to accommodate dynamic networks and time-varying membership in these frameworks. We will leave them for future research works.

## References

ACEMOGLU, D., V. M. CARVALHO, A. OZDAGLAR, AND A. TAHBAZ-SALEHI (2012): “The Network Origins of Aggregate Fluctuations,” *Econometrica*, 80, 1977–2016.

ACEMOGLU, D., A. OZDAGLAR, AND A. TAHBAZ-SALEHI (2015): “Systemic Risk and Stability in Financial Networks,” *American Economic Review*, 105, 564–608.

AHERN, K. R. (2013): “Network Centrality and the Cross Section of Stock Returns,” *SSRN Electronic Journal*, DOI: 10.2139/ssrn.2197370.

AMIHUD, Y. AND H. MENDELSON (1986): “Asset Pricing and the Bid-ask Spread,” *Journal of Financial Economics*, 17, 223–249.

AOBDIA, D., J. CASKEY, AND N. B. OZEL (2014): “Inter-industry Network Structure and the Cross-predictability of Earnings and Stock Returns,” *Review of Accounting Studies*, 19, 1191–1224.

BAKER, S. R., N. BLOOM, AND S. J. DAVIS (2016): “Measuring Economic Policy Uncertainty,” *The Quarterly Journal of Economics*, 131, 1593–1636.

BARBER, B. M. AND T. ODEAN (2008): “All That Glitters: The Effect of Attention and News on the Buying Behavior of Individual and Institutional Investors,” *Review of Financial Studies*, 21, 785–818.

BARROT, J.-N. AND J. SAUVAGNAT (2016): “Input Specificity and the Propagation of Idiosyncratic Shocks in Production Networks,” *The Quarterly Journal of Economics*, 131, 1543–1592.

BHATTACHARYYA, S. AND S. CHATTERJEE (2017): “Spectral Clustering for Multiple Sparse Networks,” *Biometrika*, 103, 1–28.

BINKIEWICZ, N., J. T. VOGELSTEIN, AND K. ROHE (2017): “Covariate-assisted Spectral Clustering,” *Biometrika*, 104, 361–377.

BONACICH, P. (1972): “Technique for Analyzing Overlapping Memberships,” *Sociological Methodology*, 4, 176–185.

BORGATTI, S. P. (2005): “Centrality and Network Flow,” *Social Networks*, 27, 55–71.

BROGAARD, J. AND A. DETZEL (2015): “The Asset-pricing Implications of Government Economic Policy Uncertainty,” *Management Science*, 61, 3–18.

CHEN, C. Y.-H., W. K. HRDLE, AND Y. OKHRIN (2019a): “Tail Event Driven Networks of SIFIs,” *Journal of Econometrics*, 208, 282–298.

CHEN, Y., J. FAN, C. MA, AND Y. YAN (2019b): “Inference and Uncertainty Quantification for Noisy Matrix Completion,” *Proceedings of the National Academy of Sciences*, 116, 22931–22937.

COHEN, L. AND A. FRAZZINI (2008): “Economic Links and Predictable Returns,” *The Journal of Finance*, 63, 1977–2011.

DEMIR, E., G. GOZGOR, C. K. M. LAU, AND S. A. VIGNE (2018): “Does Economic Policy Uncertainty Predict the Bitcoin Returns? An Empirical Investigation,” *Finance Research Letters*, 26, 145–149.

FAN, J., Y. FAN, X. HAN, AND J. LV (2019): “SIMPLE: Statistical Inference on Membership Profiles in Large Networks,” *arXiv preprint arXiv:1910.01734*.

GUO, L., L. PENG, Y. TAO, AND J. TU (2018): “News Co-Occurrence, Attention Spillover and Return Predictability,” *SSRN Electronic Journal*, DOI: 10.2139/ssrn.2927561.

HÄRDLE, W., C. HARVEY, AND R. REULE (2020): “Understanding Cryptocurrencies,” *Journal of Financial Econometrics*, 18, 181–208.

HERSKOVIC, B. (2018): “Networks in Production: Asset Pricing Implications,” *The Journal of Finance*, 73, 1785–1818.

HOU, A. J., W. WANG, C. Y.-H. CHEN, AND W. K. HÄRDLE (2020): “Pricing Cryptocurrency Options,” *Journal of Financial Econometrics*, 18, 250–279.

LEE, D. K. C., L. GUO, AND Y. WANG (2018): “Cryptocurrency: A New Investment Opportunity?” *The Journal of Alternative Investments*, 20, 16–40.

LEI, J. AND A. RINALDO (2015): “Consistency of Spectral Clustering in Stochastic Block Models,” *The Annals of Statistics*, 43, 215–237.

LEPSKI, O. V., E. MAMMEN, AND V. G. SPOKOINY (1997): “Optimal Spatial Adaptation to Inhomogeneous Smoothness: An Approach Based on Kernel Estimates with Variable Bandwidth Selectors,” *The Annals of Statistics*, 25, 929–947.

LIU, Y. AND A. TSYVINSKI (2018): “Risks and Returns of Cryptocurrency,” *Review of Financial Studies, Forthcoming*.

MATIAS, C. AND V. MIELE (2017): “Statistical Clustering of Temporal Networks through a Dynamic Stochastic Block Model,” *Journal of the Royal Statistical Society: Series B (Statistical Methodology)*, 79, 1119–1141.

MENZLY, L. AND O. OZBAS (2010): “Market Segmentation and Cross-predictability of Returns,” *The Journal of Finance*, 65, 1555–1580.

PENSKY, M. AND T. ZHANG (2019): “Spectral Clustering in the Dynamic Stochastic Block Model,” *Electronic Journal of Statistics*, 13, 678–709.

ROHE, K., T. QIN, AND B. YU (2016): “Co-clustering Directed Graphs to Discover Asymmetries and Directional Communities,” *Proceedings of the National Academy of Sciences*, 113, 12679–12684.

SHLEIFER, A. AND R. W. VISHNY (1997): “The Limits of Arbitrage,” *The Journal of Finance*, 52, 35–55.

TRIMBORN, S., M. LI, AND W. K. HÄRDLE (2020): “Investing with Cryptocurrencies - A Liquidity Constrained Investment Approach,” *Journal of Financial Econometrics*, 18, 280–306.

WILSON, J. D., N. T. STEVENS, AND W. H. WOODALL (2019): “Modeling and Detecting Change in Temporal Networks Via the Degree Corrected Stochastic Block Model,” *Quality and Reliability Engineering International*, 35, 1363–1378.

ZHANG, Y., E. LEVINA, AND J. ZHU (2016): “Community Detection in Networks with Node Features,” *Electronic Journal of Statistics*, 10, 3153–3178.

ZHANG, Y., M. POUX-BERTHE, C. WELLS, K. KOC-MICHALSKA, AND K. ROHE (2018): “Discovering Political Topics in Facebook Discussion Threads with Graph Contextualization,” *Annals of Applied Statistics*, 12, 1096–1123.

ZHANG, Y. AND K. ROHE (2018): “Understanding Regularized Spectral Clustering Via Graph Conductance,” in *Advances in Neural Information Processing Systems*, 10631–10640.

ZOU, H. (2006): “The Adaptive Lasso and Its Oracle Properties,” *Journal of the American Statistical Association*, 101, 1418–1429.

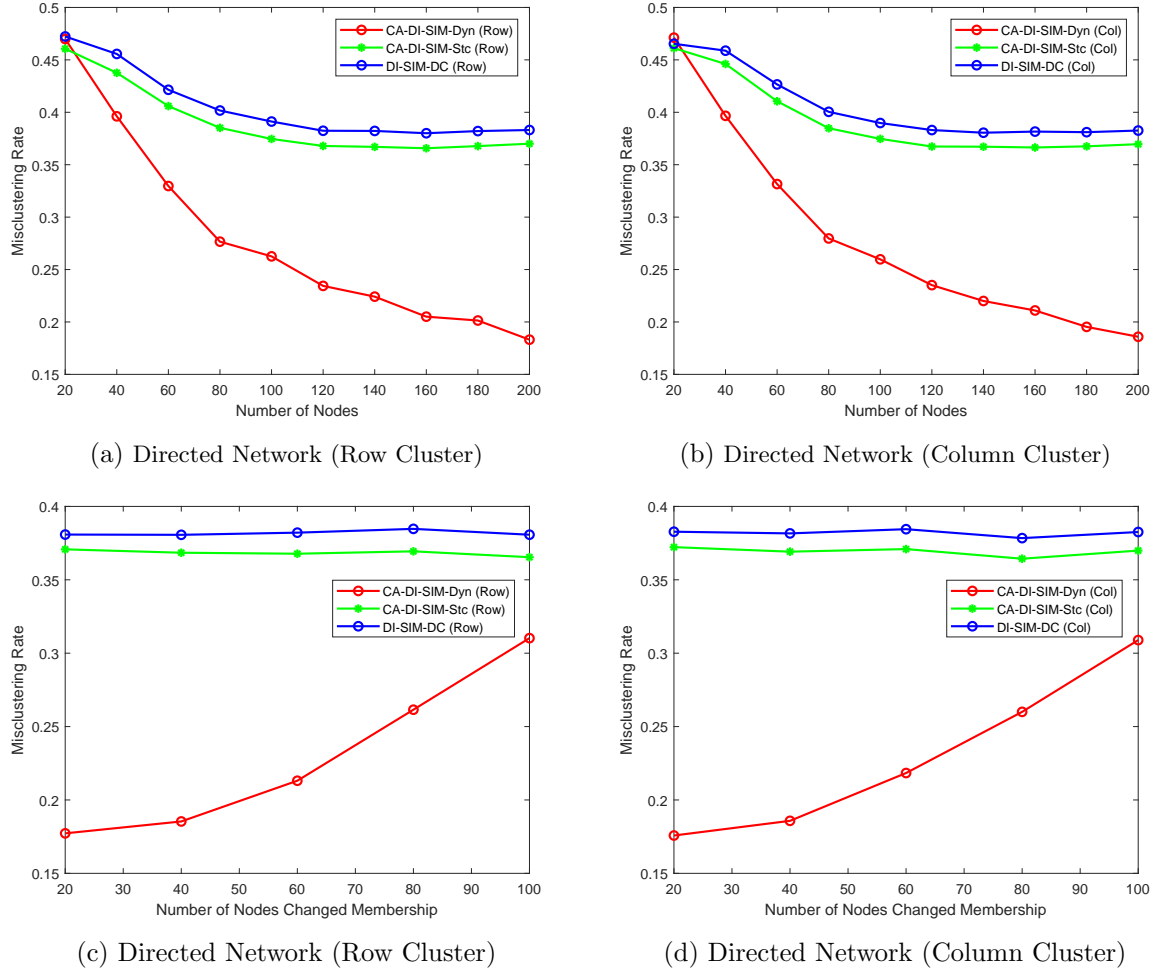


Figure 1: This figure reports the misclustering rate of different spectral clustering algorithms for networks with a growing number of vertices or with a growing number of membership changes. CA-DI-SIM-Dyn represents Algorithm 1. DI-SIM-DC is the degree-corrected DI-SIM in Rohe et al. (2016) and CA-DI-SIM-Stc is the static covariate-assisted DI-SIM method in Zhang et al. (2018). In subfigure (a) and (b), the number of nodes ( $N$ ) grows from 20 to 200 with stepsize of 20, and the number of membership changes is fixed at  $s = 10$ . In subfigure (c) and (d), the number of nodes is fixed at 200, and the number of membership changes ( $s$ ) grows from 20 to 100 with stepsize of 20. The number of periods is  $T = 10$  and the number of blocks is  $K = 4$  with block probability matrix given in equation (14). The covariates are simulated with  $R = \lfloor \ln(NT) \rfloor$  and  $X \sim U(0, 10)$ . The smoothness parameter for kernel construction is  $L = 4$ . All simulations are conducted 1000 times.

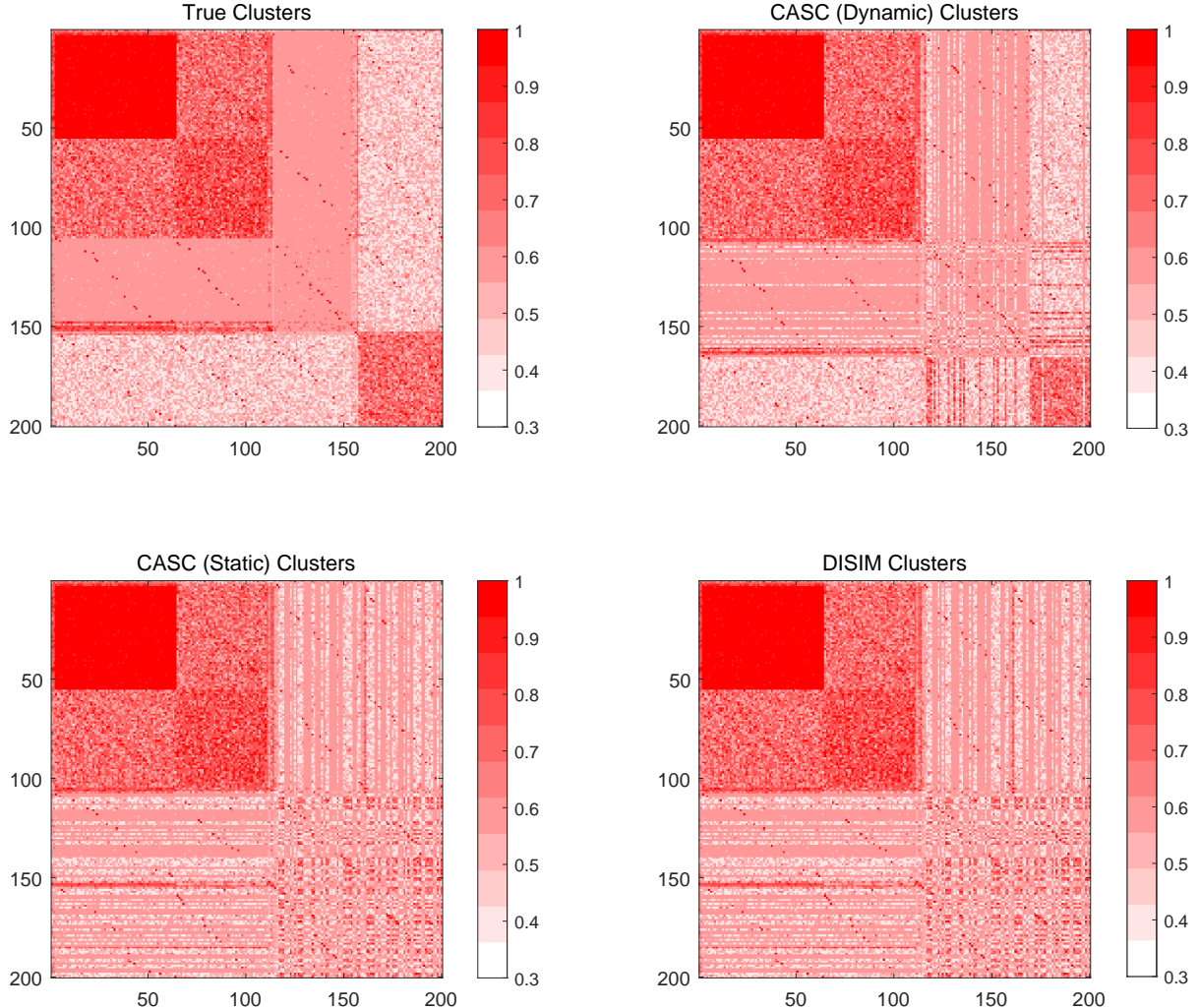


Figure 2: This figure presents the block structure of the averaged adjacency matrices according to the true clusters (simulation setting) and the estimated clusters based on different classification methods. The averaged adjacency matrix reported is  $1/6 \sum_{t=1}^6 A_t$ . The adjacency matrices have  $N = 200$  nodes with  $K = 4$  clusters. The number of periods is  $T = 10$  and the block probability matrix is given in equation (14). The covariates are simulated with  $R = \lfloor \ln(NT) \rfloor$  and  $X \sim U(0, 10)$ . The number of group member changes is fixed at  $s = 20$  and the smoothness parameter for kernel construction is  $L = 4$ . All simulations are conducted 1000 times.

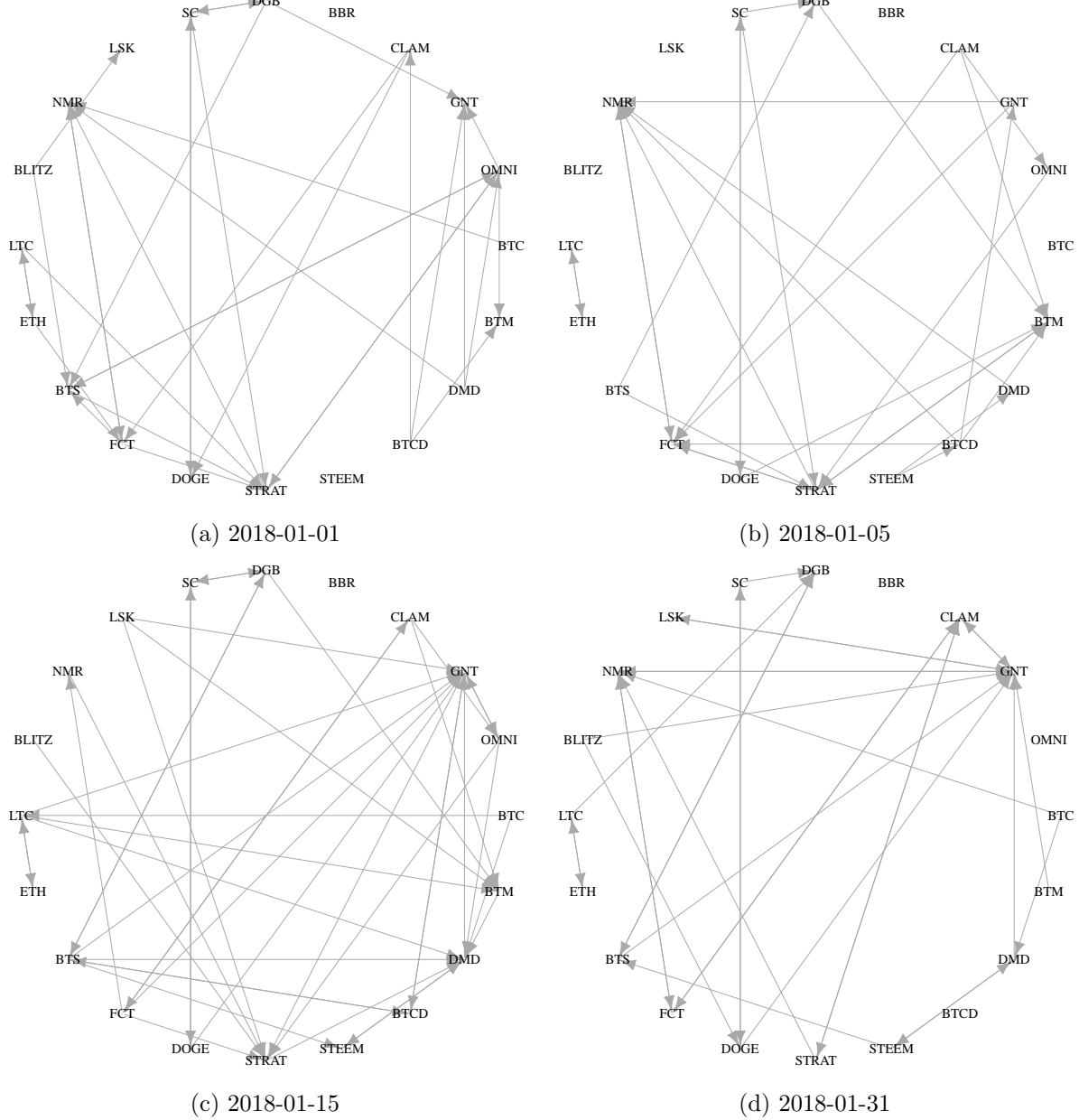
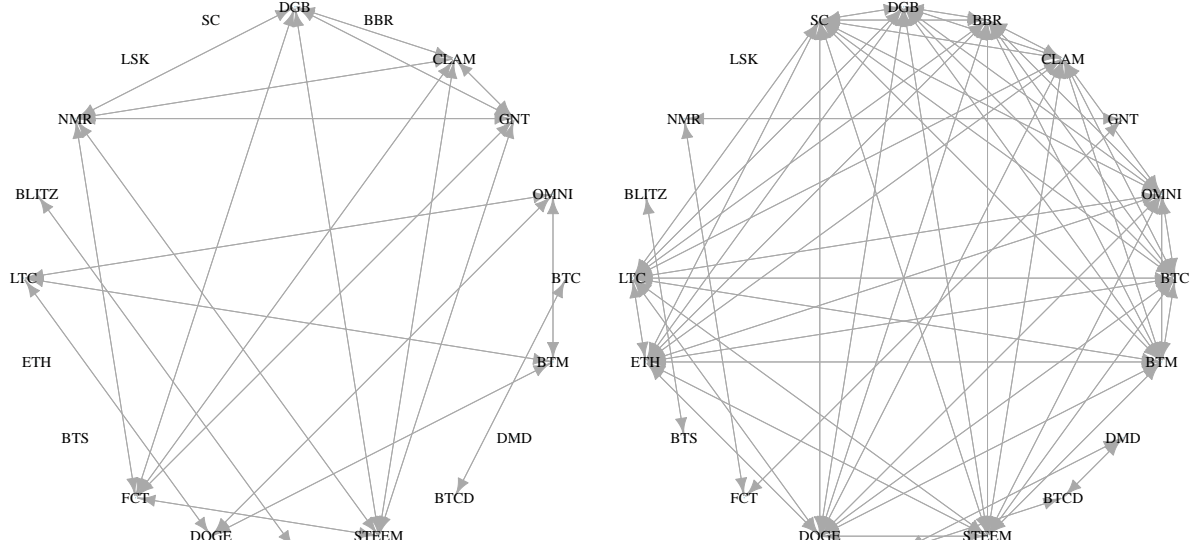
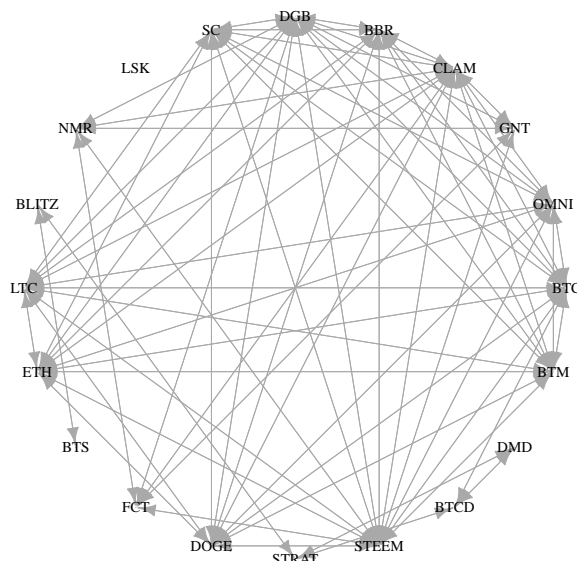


Figure 3: This figure presents the return-based cryptos network on selected dates in January 2018. We selected 20 cryptos, including BTC, ETH, LTC and other top cryptos by market capitalization as of December 31, 2017. We obtained the connections from the predictive regression  $r_{i,t+1}^s = \alpha_i + \sum_{j=1, j \neq i}^{N-1} b_{i,j} r_{j,t}^s + \epsilon_{i,t}$ , where  $r_{i,t}^s$  is the standardized daily return on crypto  $i$  and  $N$  is the total number of cryptos. Only the cryptos selected by adaptive LASSO will be linked to crypto  $i$ . An arrow from crypto A to crypto B means crypto A's return can predict the crypto B's return.



(a) Algorithm

### (b) Proof Types



### (c) Combined Fundamentals

Figure 4: This figure depicts the contract-based cryptos network. We connect two cryptos with double-arrowed edges if they share the same fundamental technology, i.e., algorithm and proof types.

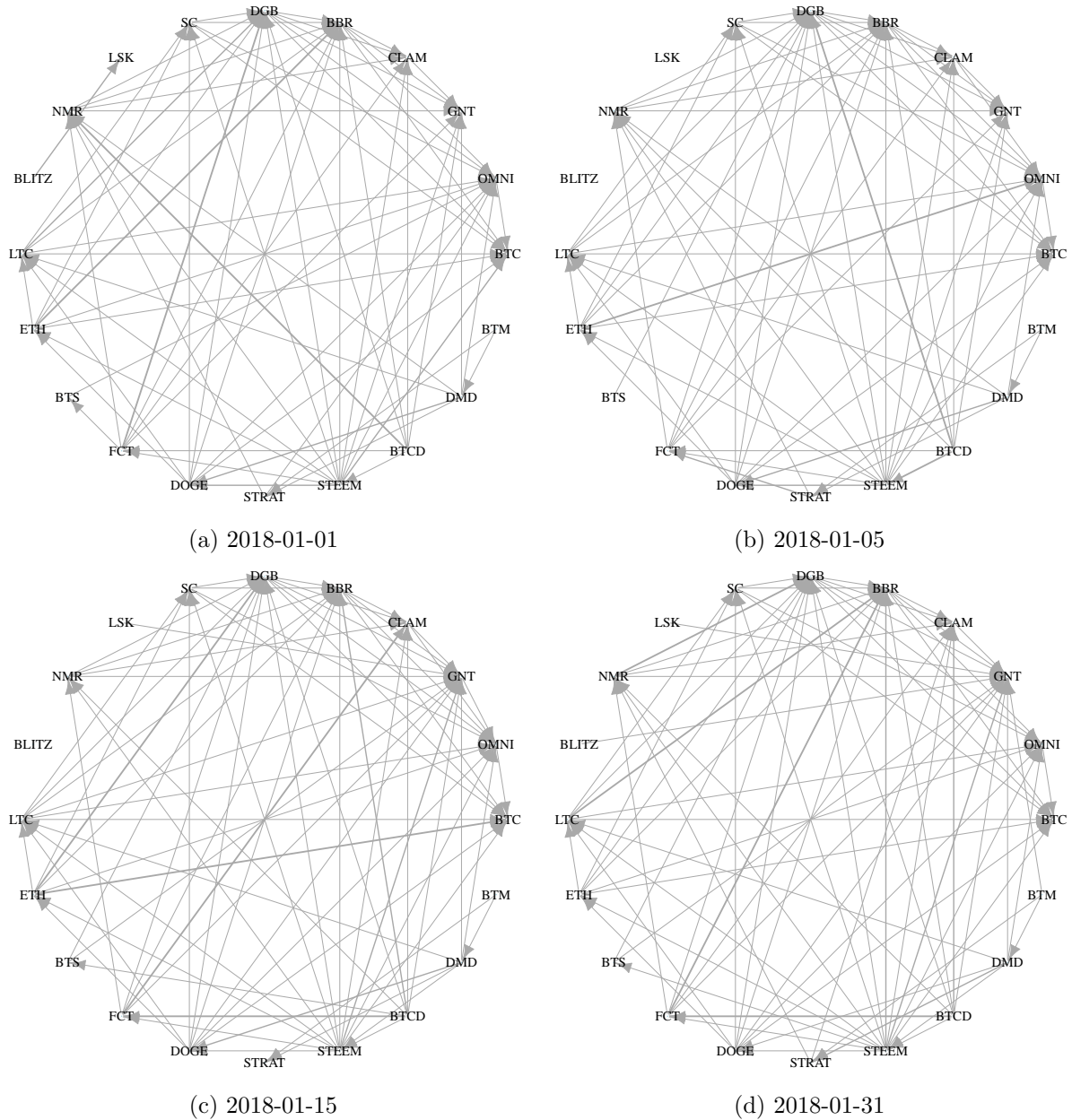


Figure 5: This figure depicts the combined dynamic cryptos network, in which cryptos are linked either by return cross-predictability or by fundamental similarity.

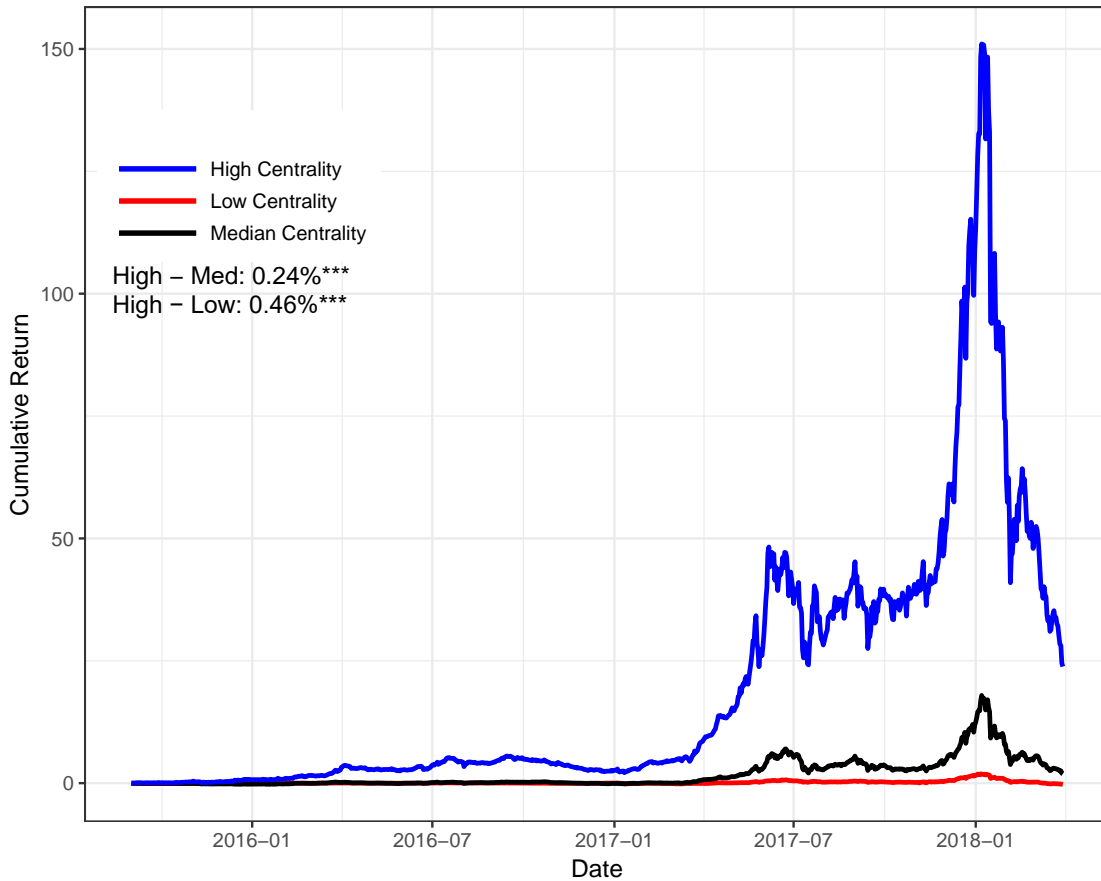


Figure 6: This figure depicts the cumulative portfolio return of the high-, median-, and low-centrality groups. The centrality is computed as the eigenvector centrality of the similarity matrix which optimally combines the return inferred adjacency matrix, algorithm-based covariates and prootype-based covariates. The cryptos in the highest (lowest) quintile are regarded as long (short) leg and the rest cryptos are regarded as the middle leg. The blue curve plots the cumulative return of highest centrality portfolio, the black curve plots the cumulative return of the middle group and the red curve plots the cumulative return of the lowest centrality group. The sample period spans from August 31, 2015 to March 31, 2018.

Table 1: Representative Cryptos of Groups Estimated by DISIM and by Dynamic CASC.

Group ID	Group 1	Group 2	Group 3	Group 4
DISIM Rohe et al. (2016)	BBR	<b>BTC</b>	BLITZ	BTCD
	LSK	DGB	STEEM	CLAM
	DOGE	<b>LTC</b>	SC	GNT
	<b>ETH</b>	NMR	BTS	
	OMNI	DMD		
	BTM	STRAT		
Dynamic CASC	BBR	BLITZ	BTS	BTCD
	<b>BTC</b>	DGB	DOGE	BTM
	CLAM	LSK	<b>ETH</b>	DMD
	GNT	NMR	FCT	STEEM
	OMNI	SC	<b>LTC</b>	STRAT

Table 2: Within- and Cross-group Connections using DISIM and Dynamic CASC

This table reports the in-sample connections for the within- and cross- group members. Panel A reports the average return-based connection across the sample period. Panels B and C report the algorithm-inferred connections and proof-type-inferred connections, respectively. Each trading day, we compute the average correlation, the algorithm linkage and the prooftype linkage for both the within- and cross group members in the past 60 days according to today's group membership. The upper part reports the results based on the benchmark model of [Rohe et al. \(2016\)](#) and the lower part reports the results of the dynamic CASC.

	Panel A: Return			Panel B: Algorithm			Panel C: Proof Types		
	Within	Cross	Diff.	Within	Cross	Diff.	Within	Cross	Diff.
<b>Panel A: DISIM by <a href="#">Rohe et al. (2016)</a></b>									
Group 1	0.033	0.051	-0.018	0.252	0.204	0.048	0.252	0.233	0.020
Group 2	0.084	0.074	0.010	0.216	0.198	0.018	0.282	0.242	0.040
Group 3	0.086	0.075	0.011	0.215	0.196	0.019	0.284	0.242	0.042
Group 4	0.084	0.073	0.011	0.216	0.197	0.019	0.283	0.242	0.042
Overall	0.072	0.068	0.004	0.225	0.199	0.026	0.275	0.239	0.036
<b>Panel B: Dynamic CASC</b>									
Group 1	0.064	0.058	0.006	0.232	0.202	0.030	0.270	0.236	0.034
Group 2	0.063	0.057	0.007	0.243	0.203	0.041	0.277	0.236	0.041
Group 3	0.065	0.057	0.008	0.240	0.202	0.038	0.277	0.236	0.042
Group 4	0.065	0.057	0.009	0.240	0.202	0.038	0.277	0.236	0.041
Overall	0.065	0.057	0.007	0.239	0.202	0.037	0.275	0.236	0.039

Table 3: Within- and Cross-group Cryptos' Average Return Correlations by Dynamic CASC.

This table reports the out-of-sample performance of within- and cross-group average return correlation based on dynamic CASC. Each trading day, we balance the portfolio according to the today's clustering results and calculate the within- and cross-group return correlations in the next 60 trading days. The number in brackets below are the  $t$ -statistics, which are adjusted by the Newey-West lags(4) method. The sample period spans from August 31, 2015 to March 31, 2018.

	Within Group	Cross Group	Diff.
Group 1	0.169 (7.626)	0.154 (7.423)	0.014 (6.856)
Group 2	0.179 (8.077)	0.154 (7.423)	0.021 (6.077)
Group 3	0.181 (8.191)	0.157 (7.506)	0.021 (10.374)
Group 4	0.188 (8.114)	0.157 (7.416)	0.027 (5.607)
Overall	0.188 (7.697)	0.157 (7.381)	0.021 (6.331)

Table 4: Average Future Returns of the Cross-sectional Portfolios by Centrality Sorting.

This table reports the average future return for quartile portfolios sorted by the centrality measure. The centrality is computed as the eigenvector centrality of the similarity matrix which optimally combines the return inferred adjacency matrix, algorithm-based covariates and prooftype-based covariates. In the end of each trading day, we balance the portfolio according to today's centrality score and long the cryptos with high centrality score and short the cryptos with low centrality score. The  $t$ -statistics in parentheses are computed based on standard errors with a Newey-West lags(4) adjustment. The sample period spans from August 31, 2015 to March 31, 2018.

Centrality	$Ret_{t+1}$	$Ret_{t+2}$	$Ret_{t+3}$	$Ret_{t+4}$	$Ret_{t+5}$	$Ret_{t+6}$	$Ret_{t+7}$
Low	0.00%	0.04%	-0.03%	-0.02%	0.03%	0.04%	0.08%
2	0.13%	0.15%	0.18%	0.19%	0.16%	0.17%	0.13%
3	0.36%	0.34%	0.28%	0.36%	0.37%	0.28%	0.30%
High	0.39%	0.36%	0.47%	0.38%	0.35%	0.42%	0.39%
High - Low	0.39%	0.33%	0.51%	0.40%	0.32%	0.39%	0.31%
$t$ -statistic	(3.47)	(3.10)	(4.23)	(3.40)	(2.77)	(3.37)	(2.73)

Table 5: Portfolio Returns: Trading Volume, Investor Attention, and Macro Uncertainty

This table reports the quartile portfolio returns sorted by the centrality measure for cryptos with high and low trading volume, in high- and low-investor-attention periods, or under high- and low-macro-uncertainty circumstances. *t*-statistics in parentheses are computed based on standard errors with Newey-West lags(4) adjustment. The sample period spans from August 31, 2015 to March 31, 2018.

Centrality	Trading Volume		Investor Attention		Macro Uncertainty	
	Low	High	Low	High	Low	High
Low	0.05%	-0.04%	0.04%	0.01%	0.01%	0.01%
2	0.16%	0.27%	0.11%	0.21%	0.02%	0.26%
3	0.38%	0.12%	0.46%	0.32%	0.22%	0.54%
High	0.56%	0.28%	0.39%	0.46%	0.32%	0.49%
High - Low	0.51%	0.33%	0.35%	0.45%	0.31%	0.48%
<i>t</i> -statistic	(3.62)	(2.73)	(2.27)	(3.06)	(2.23)	(2.71)